Schutt et al., 2018, Moho temperature and mobility of lower crust in the western United States: Geology, https://doi.org/10.1130/G39507.1.

Supplementary Text

1.0 Calculation of Temperatures

1.1 Elastic/Compositional Effects

To convert Pn velocity to temperature, a reference mantle composition must first be assumed. We use measurements from a synthetic fertile spinel lherzolite (MM3) created from xenolith separates of a Kilbourne Hole nodule (Lesher and Baker, 1997; Baker and Stolper, 1994). We chose a measured composition over self-consistent thermodynamical models for three reasons: 1) extrapolations of thermodynamical values outside the compositional, pressure, and temperature range of measurements may lead to unknown errors; 2) the method of Schutt and Lesher (2006) more readily allows estimation of the effects of uncertainty in mineral physics parameters such as bulk and shear moduli; and, 3) unlike the polynomial fits of Schutt and Lesher (2006; 2010), most self-consistent thermodynamical models (e.g., Perple_X, Connolly, 1990) use a 3rd order Eulerian strain approximation which cannot reproduce the significant 2nd pressure derivatives in the shear and bulk moduli of enstatite (Flesch et al., 1998). The polynomial fit approximation of Schutt and Lesher (2006) does. To account for uncertainty in composition, it is arbitrarily assumed that lherzolite mantle mineral modes have a 1-sigma uncertainty of 2%, and mineral mode end-member proportions (e.g. forsterite and fayalite) also have a 2% uncertainty. We assume spinel is the stable aluminous phase over the range of pressures associated with Pn depths.

A limitation of this method is that subsolidus mineralogical variations are not considered. Likely the most important effect is the opening of the pyroxene solvus as temperature decreases, which affects the relative amounts and compositions of the mineral modes clinopyroxene and orthopyroxene. Schutt and Lesher (2006) examined subsolidus effects and found that while density does change somewhat with decreasing temperature, velocity change is negligible.

We recognize that the mantle is not compositionally homogeneous, but we infer that the large velocity variations found in lithospheric mantle (Shen et al., 2013; Buehler and Shearer, 2012; Buehler and Shearer, 2014; Buehler and Shearer, 2017) must be primarily due to temperature variations because no plausible compositional anomaly can produce the full range of variations observed seismically (Afonso and Schutt, 2012; James et al., 2004; Schutt and Lesher, 2006). Possible compositional effects are discussed in the main text.

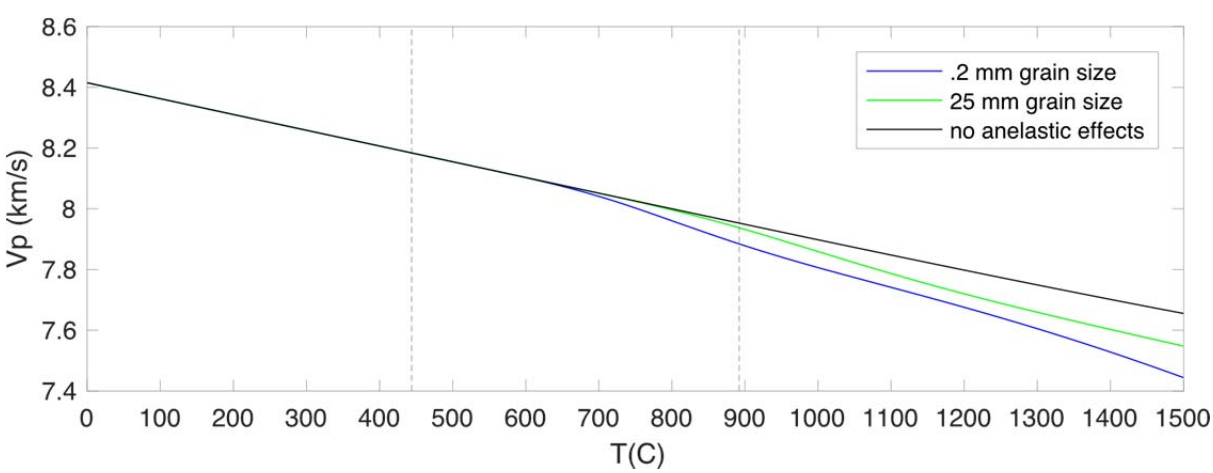

Figure DR1: Pn velocity at 40 km depth, as a function of temperature. The dashed lines span the range of 95% of the inferred temperatures in the model.

1.2 Anelastic Effects

As discussed in the main text, the grain size-sensitive approach of Jackson and Faul (2010) is used to calculate anelastic effects. First, the elastic moduli and the density are calculated for MM3 at the pressure and temperature of interest. Then, the relaxed shear modulus is calculated from Jackson and Faul (2010) as a reduction from the elastic shear modulus and assuming that bulk modulus attenuation is 0. V_P is then calculated using the relaxed shear modulus, the elastic bulk modulus, and the density (Figure DR1).

2.0 Uncertainties

2.1 Mineral Moduli and Anelasticity

To estimate uncertainty in the final temperatures, we consider the scatter in inter-laboratory mineral physics parameter measurements (Schutt and Lesher, 2006); assume the proportion of mineral modes spinel, olivine, clinopyroxene, and orthopyroxene is normally distributed and varies by a standard deviation of 2% from MM3 composition (as described above, and such that the total modal volumes add to 100%); assume grain size varies between .2-25 mm (Armienti and Tarquini, 2002); and assume 1-σ crustal thickness uncertainties of 7 km. To our knowledge, no study estimating temperature variations in lithospheric mantle has formally propagated uncertainties in such a manner. However, it must be emphasized that the anelastic effects are particularly uncertain, since grain sizes are not well-constrained and no studies exist on peridotite anelasticity at mantle conditions**.**

No work yet considers the effects of a grain size distribution on mantle anelasticity, so a particular grain size distribution cannot be considered in our modelling, but it is worth considering how grain sizes might vary in the lithospheric mantle. While grain sizes are often mentioned in petrographic studies, few studies have looked at them in a systematic manner. Probably the most quantitative investigation is that of Armienti and Tarquini (2002), who found a power law distribution of grain sizes, $N(D) = CD^{-m}$, where $N(D)$ is the number of crystals per unit size per unit volume, D is the equivalent diameter of the crystals, C is a constant, and m is the power law exponent. In this study, m varied between about 2.4 to 3.8; however, given that anelasticity is primarily a grain boundary effect, the distribution of grain surface area is a more salient quantity. This is the 2nd order moment of the grain size distribution (scaled by a constant): $N(A) = C_A D^{-m+2}$, where $N(A)$ is the number of crystals per unit surface area per unit volume and C_A is a new constant. The power law exponent for grain surface area distribution thus varies between roughly 0.4 to 1.8, flattening out the distribution, and increasing the relative importance of the larger grains relative to the smaller grains, although smaller grains would still dominate a surface area distribution.

With this in mind, the effects of anelasticity uncertainty are approximated by using the temperatures that result from the 0.2 mm and 25 mm grain sizes as the upper and lower bounds of the temperature uncertainty due to anelasticity. The mean of these is assumed to be the mostly likely temperature, based on the consideration that the surface area effects due to a grain size distribution are near to being flat (m is not too far from 0). One of the advantages of using the Pn phase, which travels through relatively cool mantle, is that the effects of anelasticity on temperature are fairly

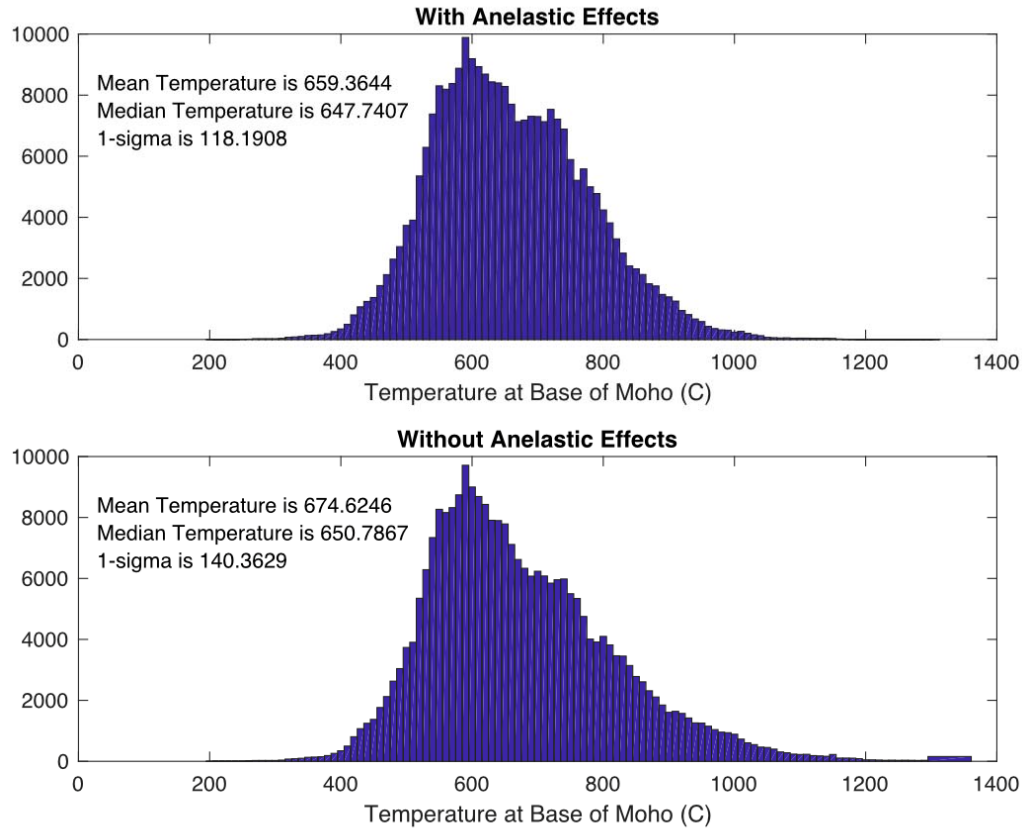

Figure DR2: Histogram showing temperatures within the western U.S. with (top) and without (bottom) an anelastic correction.

small overall. Adding in the mean anelastic correction lowers the median temperature in our model from 651°C to 648°C (Figure DR2). It also reduces the spread of velocities somewhat by compressing the range of temperatures needed to explain the lowest velocities. The 0.2 mm grain size reduces the median temperature in our model to 645°C, whereas the 25 mm grain size produces a median model temperature of 651°C (Figure DR3).

Figure DR4 shows the estimated uncertainties as a function of depth and pressure, which gives an indication when anelastic effects play a role in the calculated temperatures.

2.2 Crustal Thickness

For self-consistency, we use the crustal thickness estimates from Buehler and Shearer (2017) (Figure DR5) and estimate that the uncertainty in Pn depth is ± 7 km. The effect of this on the ability to estimate temperature from Pn velocity is shown in Figure DR5, with the mean temperature uncertainty due to crustal thickness uncertainty being 26°C.

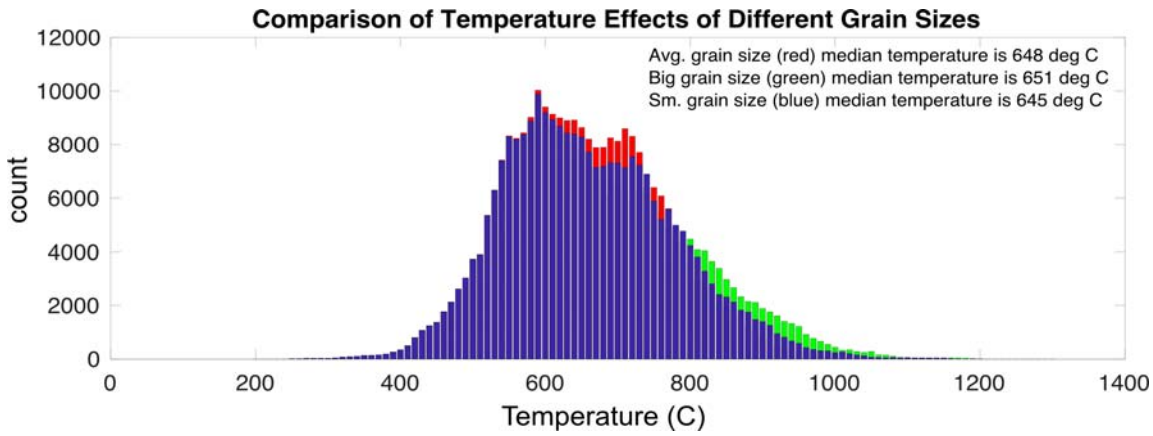

Figure DR3: Effect of grain size on estimated temperature.

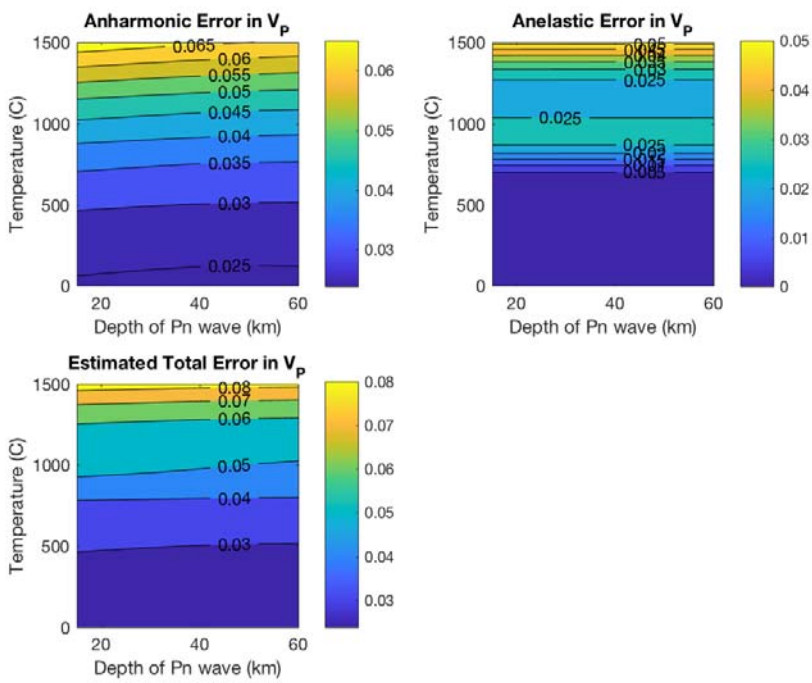

Figure DR4: Estimated elastic and anelastic uncertainty as a function of temperature and pressure

2.3 Velocity Uncertainty

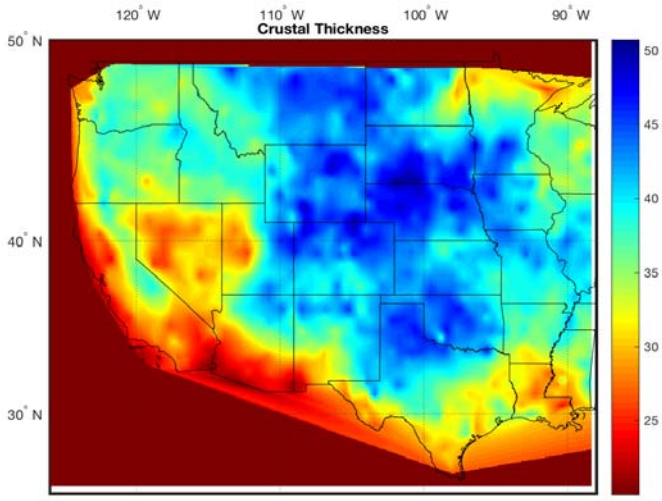

Figure DR5: Crustal thickness (km) model.

A notable challenge in inverse theory is determining uncertainty in model parameters. In this study, an ad hoc approach to estimating Pn tomography uncertainties is undertaken. Velocity inversion results from a 600°C starting model are compared to those for an 800°C starting model, a range chosen because these temperatures bound the temperature estimates for most of the western U.S. Where model parameters are well-resolved, for instance due to many crossing rays, the starting model should have little effect on the final model. Elsewhere, the starting model and the effects of inversion regularization will play a larger role in the outcome. Most of the study area has *Vp* uncertainties of 0.01-0.04 km/s, and 0.08 km/s is a reasonable bound for the well-resolved area of the study (Figure DR6). Figure DR7 shows the resulting temperature uncertainty.

2.4 Total Uncertainty

When all of the uncertainties are combined, the mean uncertainty in temperature for the region of study is 77°C (Figure DR8).

2.5 Deviations from the Null Hypothesis

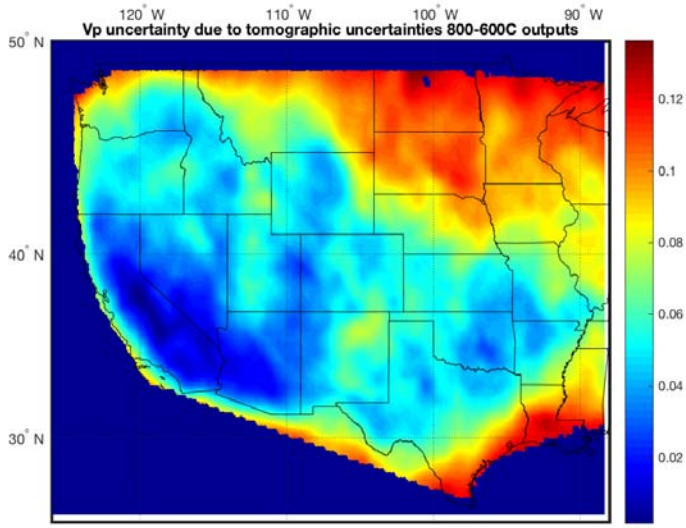

Figure DR6: Difference in inversion output velocity between an 800°C and a 600°C starting model.

These calculations are based on the study's null hypothesis that the mantle is of uniform composition. No study that we know of examines the full range of compositional variations observed in mantle xenoliths. Indeed, the ability to thermodynamically calculate the stable mineral assemblage and accurately estimate the velocity associated with a mantle xenolith for a given upper mantle temperature and pressure is limited to a relatively small range of whole rock major element compositions. Limited mineral physics studies suggest that metasomatic or hydrous lithologies may produce lower velocities relative to lherzolite. The relative plausibility of such cases is presented in the main text discussion. However, we note two cases where metasomatic reductions in velocity might be expected, but are not observed.

Pn velocity variations are not observed along the Midcontinent Rift, where one might expect a compositional anomaly, but no thermal perturbation (Stein et al., 2016). Also estimated temperatures under the Lucite Hills volcanic center (~3.0-0.89 Ma) in southwestern Wyoming are quite low, and yet this is inferred from petrology and geochemistry to be an area of mantle metasomatism metasomatism (Mirnejad and Bell, 2006). Consequently, while the possibility of unusual mineral assemblages must be considered when interpreting the results of this study, the consistency of the Pn tomography with heatflow variations (Blackwell et al., 1991), deeper mantle velocity structures (Schmandt and Lin, 2014), and the lack of clear correlations between metasomatic locations and low velocity features, suggests the null hypothesis broadly holds.

Also, while Buehler and Shearer (2017) correct for deviations of the Pn wave from a simple head wave approximation, their approach is not a full-waveform inversion, and velocities may be misestimated in locations where a more ray theoretical approach over simplifies wave propagation effects. In particular, the Sierra Nevada seem to have some unusual Pn propagation paths, including a shadow zone (Jones et al., 1994).

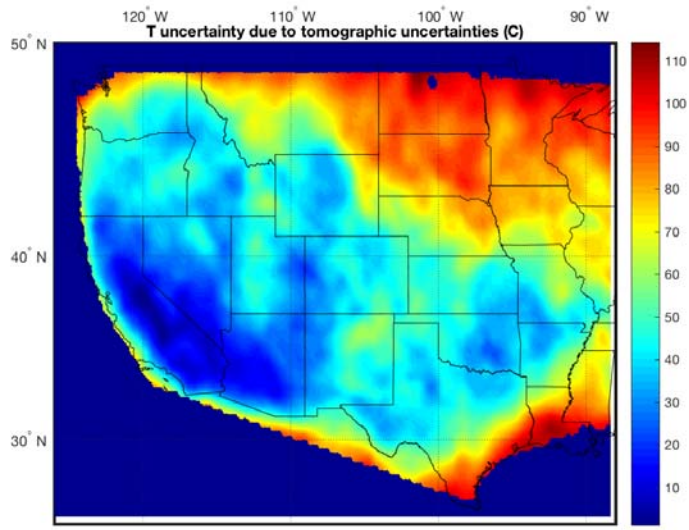

Figure DR7: Velocity difference of Figure DR6 mapped to temperature difference.

3.0 Calculation of Effective Viscosities

We assume a strain rate of 10^{-14} s^{-1} for the results shown in Fig. 4 and discussed in the text. We examined the effects of other strain rates (not shown), but one can generalize the viscosities shown by recognizing that effective viscosity decreases with increasing strain rate as $\eta_{eff} \propto \dot{\varepsilon}^{(1-n)/n}$, where *n* is the power-law exponent of the creep law. The calculations used both the diffusion and dislocation creep laws for each mineral, taking the lesser yield strength and viscosity of the two, although practically the diffusion creep strength is never smaller within the lithosphere unless (unlikely) grain sizes of less than 100 μm are assumed. Observations of seismic anisotropy in this depth range (Buehler and Shearer, 2014; Buehler and Shearer, 2017) would suggest that dislocation creep is the dominant mechanism. The flow laws used here, from the compilation of Bürgmann and Dresen (2008), all were derived using Paterson-type apparati and synthetic minerals to guarantee maximum control of the individual contributions from composition, water fugacity, grain size, etc. The temperature used was the unperturbed estimate of Moho temperature depicted in Fig. 2. This temperature represents the physical state near the centroid of the Frechet kernels of the Pn phase arrivals used in the tomographic inversion of Buehler and Shearer (2017), which we estimate to be about 2 km below the actual Moho. Consequently, the dry olivine effective viscosity (Fig. 4e) will be an accurate representation for that depth, but lower crustal effective viscosities are slightly underestimated. In geotherms derived using this temperature product, the mean gradient at ~40 km depth is 12°C/km, so the temperature of the lowermost crust is about 24°C lower than represented in Fig. 4a-d and f. Visual inspection of the differences between Fig. 4 and a version of Fig. 4 generated assuming a 25°C lower temperature

suggests that the lower temperature increases effective viscosity by up to a factor of two, but on the logarithmic color scale of Fig. 4, the resulting differences are visually very subtle. Pressure was derived from the crustal thickness (Figure DR5) assuming a mean crustal density of 2960 kg m^{-3}. Water fugacity used to calculate "wet" (saturated) rheologies is pressure-dependent and calculated from the mineral equations of state.

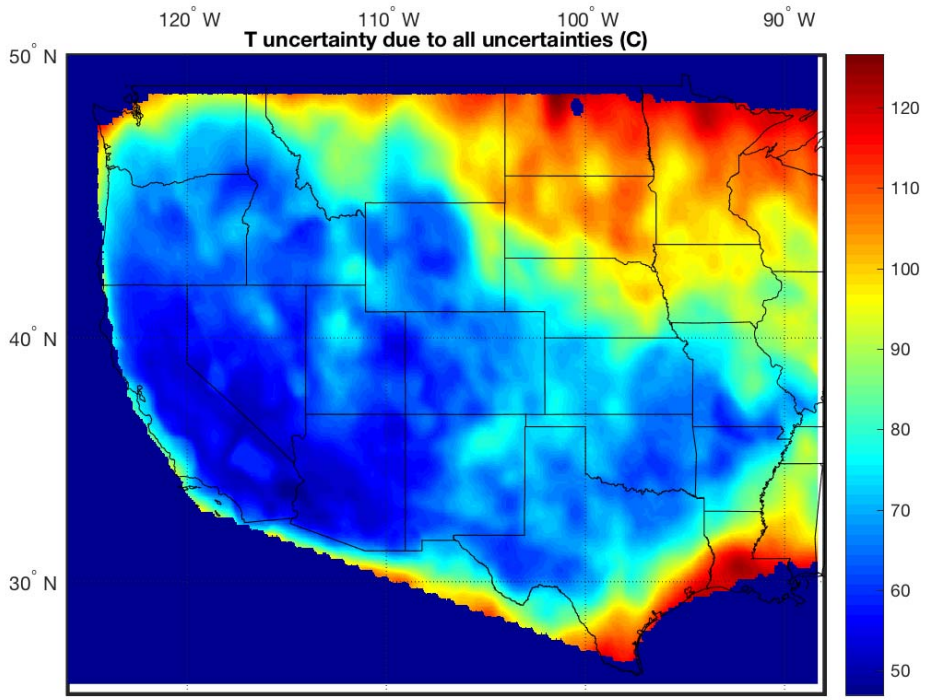

Figure DR8: Total estimated uncertainty given the null hypothesis of relatively constant lherzolitic composition, after elastic, anelastic, crustal thickness, and tomographic uncertainties are considered.

Temperature Model

The temperature model can be found at: https://doi.org/10.17611/DP/EMCMTWUS17, and contains latitude, longitude, temperature (°C), crustal thickness, and temperature uncertainty.

References Cited

Afonso, J.C., and Schutt, D.L., 2012, The effects of polybaric partial melting on density and seismic velocities of mantle restites: Lithos v. 134-135, p, 289–303.

Armienti, P., and Tarquini, S., 2002, Power law olivine crystal size distributions in lithospheric mantle xenoliths: Lithos v. 65, p, 273–285.

Baker, M.B., and Stolper, E.M., 1994, Determining the composition of high-pressure mantle melts using diamond aggregates: Geochimica et Cosmochimica Acta v. 58, p, 2811–2827.

Blackwell, D.D., Steele, J.L., and Carter, L.C., 1991, Heat flow patterns of the North American continent: A discussion of the DNAG geothermal map of North America: Neotectonics of North America: Geological Society of America DNAG Decade Map v. 1, p, 423–437.

Buehler, J.S., and Shearer, P.M., 2012, Localized imaging of the uppermost mantle with USArray Pn data: J. Geophys. Res. v. 117, p, n/a.

Buehler, J.S., and Shearer, P.M., 2014, Anisotropy and Vp/Vs in the uppermost mantle beneath the western United States from joint analysis of and phases: J. Geophys. Res. Solid Earth v. 119, p, 1200–1219.

Buehler, J.S., and Shearer, P.M., 2017, Uppermost mantle seismic velocity structure beneath USArray: J. Geophys. Res. Solid Earth v. 122, p, 436–448.

Bürgmann, R., and Dresen, G., 2008, Rheology of the Lower Crust and Upper Mantle: Evidence from Rock Mechanics, Geodesy, and Field Observations: Annu. Rev. Earth Planet. Sci. v. 36, p, 531–567.

Connolly, J.A.D., 1990, Multivariable phase diagrams: an algorithm based on generalized thermodynamics.: Am J Sci v. 290, p, 666–718.

Flesch, L.M., Li, B., and Liebermann, R.C., 1998, Sound velocities of polycrystalline MgSiO3-orthopyroxene to 10 GPa at room temperature: American Mineralogist v. 83, p, 444–450.

Jackson, I., and Faul, U.H., 2010, Grainsize-sensitive viscoelastic relaxation in olivine: Towards a robust laboratory-based model for seismological application: Physics of the Earth and Planetary Interiors v. 183, p, 151–163.

James, D.E., Boyd, F.R., Schutt, D., Bell, D.R., and Carlson, R.W., 2004, Xenolith constraints on seismic velocities in the upper mantle beneath southern Africa: seismic velocigties from mangtle xenoliths: Geochem. Geophys. Geosyst. v. 5, p, n/a.

Jones, C.H., Kanamori, H., and Roecker, S.W., 1994, Missing roots and mantle “drips”: Regional Pn and teleseismic arrival times in the southern Sierra Nevada and vicinity, California: Journal of Geophysical Research: Solid Earth v. 99, p, 4567–4601.

Lesher, C.E., and Baker, M.B., 1997, Near-solidus phase relations of a mantle peridotite at 3.6–5 GPa: Eos Trans. AGU

Mirnejad, H., and Bell, K., 2006, Origin and Source Evolution of the Leucite Hills Lamproites: Evidence from Sr-Nd-Pb-O Isotopic Compositions: Journal of Petrology v. 47, p, 2463–2489.

Schmandt, B., and Lin, F.-C., 2014, P and S wave tomography of the mantle beneath the United States: Geophys. Res. Lett. v. 41, p, 6342–6349.

Schutt, D.L., and Lesher, C.E., 2006, Effects of melt depletion on the density and seismic velocity of garnet and spinel lherzolite: J. Geophys. Res. v. 111, p, B05401.

Schutt, D.L., and Lesher, C.E., 2010, Compositional trends among Kaapvaal Craton garnet peridotite xenoliths and their effects on seismic velocity and density: Earth and Planetary Science Letters v. 300, p, 367–373.

Shen, W., Ritzwoller, M.H., and Schulte-Pelkum, V., 2013, A 3-D model of the crust and uppermost mantle beneath the Central and Western US by joint inversion of receiver functions and surface wave dispersion: J. Geophys. Res.-Solid Earth v. 118, p, 262–276.

Stein, S., Stein, C., Kley, J., Keller, R., Merino, M., Wolin, E., Wiens, D., Wysession, M., Al-Equabi, G., Shen, W., Frederiksen, A., Darbyshire, F., Jurdy, D., Waite, G., Rose, W., Vye, E., Rooney, T., Moucha, R., and Brown, E., 2016, New Insights into North America's Midcontinent Rift: Eos v. 97